Spring 2016

Estimating the capture efficiency of a vegetative environmental buffer using Lidar

William Brandon Willis
University of Iowa

ESTIMATING THE CAPTURE EFFICIENCY OF A VEGETATIVE ENVIRONMENTAL BUFFER USING LIDAR

by

William Brandon Willis

A thesis submitted in partial fulfillment
of the requirements for the Master of Science
degree in Civil and Environmental Engineering in the
Graduate College of
The University of Iowa

May 2016

Thesis Supervisor: Professor William E. Eichinger

Graduate College
The University of Iowa
Iowa City, Iowa

CERTIFICATE OF APPROVAL

_____

MASTER'S THESIS

_____

This is to certify that the Master's thesis of

William Brandon Willis

has been approved by the Examining Committee for
the thesis requirement for the Master of Science degree
in Civil and Environmental Engineering at the May 2016 graduation.

Thesis Committee: _____
William E. Eichinger, Thesis Supervisor

_____
John H. Prueger

_____
Corey D. Markfort

ACKNOWLEDGEMENTS

First, I must thank the organizers, scientists, and technicians of the field campaign: Hong Li, Bill Eichinger, John Prueger, Cathleen Hapeman, Mike Buser, Sean Plenner, Warren Clarida, Steve Browne, Peter Downey, Jerry Hatfield, Gregory Holt, Alba Torrents, and Qi Yao. An impressive collaborative effort was needed to accomplish the experiment, and all involved were superb. I also thank Bill, John, Hong, Mike, and Cathleen for their efforts in editing the material contained in this thesis.

Thank you, Sean, for showing me the ropes in the lidar lab.

Special thanks to Bill, my advisor, for always encouraging me and remaining patient throughout my time at Iowa. He allowed me to make mistakes, yet he always trusted me. To a large degree I credit Bill for developing my own self-reliance and resourcefulness. Bill, thank you for everything you have taught me.

I must thank my parents: for making sacrifices so I could come to Iowa and for supporting me in everything I do. Thank you Mom, Dad, David, and Lisa.

Finally, and most expressively, I acknowledge Marissa, who has been by my side through the whole process. She shows me how to be sincere and tough every day. Thank you Riss, for being my inspiration and for always fact-checking me.

ABSTRACT

Particulate matter expelled from tunnel-ventilated animal feeding operations (AFOs) is known to transport malodorous compounds. As a mitigation strategy, vegetative environmental buffers (VEBs) are often installed surrounding AFOs in order to capture particulates and induce lofting and dispersion. Many farmers are or are interested in implementing VEBs, yet research supporting their efficacy remains sparse.

Currently, point measurements, often combined with models, are the primary means by which emission rates from AFOs and VEB performance has been investigated. The existing techniques lack spatial resolution and fail to assign the observed particulate reduction to capture, lofting, or dispersion.

In recent years, lidar has emerged as a suitable partner to point measurements in agricultural research. Lidar is regarded for its ability to capture entire plume extents in near real time. Here, a technique is presented for estimating the capture efficiency of a VEB using lidar. An experiment was conducted in which dust was released upwind of a VEB at a known rate, and the emission rate downwind of the VEB was estimated using an elastic scanning lidar. Instantaneous lidar scans showed periodic lofting well above the VEB, but when scans were averaged over several hours, the plumes appeared Gaussian. The experiment revealed a capture efficiency ranging from 21-74%, depending on the time of day. The methodology presented herein addresses deficiencies in the existing techniques discussed above, and the results presented add to the lacking body of research documenting VEB capture efficiency.

PUBLIC ABSTRACT

Over the last few decades, advances in mechanical, biological, and chemical technologies have allowed single farms to manage larger numbers of animals. As a result, every sector of animal husbandry has shifted toward large-scale production. Large-scale production increases efficiency and reduces cost, but the practice concentrates animals onto smaller plots of land, concentrating sources of animal-derived pollution. Many pollutants, such as ammonia and dust, are emitted into the air in high concentrations and carried downwind to neighboring communities. Research has even shown that odorous compounds are carried by dust particles, and if we can limit the amount of dust emitted, then we can limit odor problems in many rural areas.

Many farmers are interested in building tree buffers surrounding their facilities to help reduce the impact of odors to neighboring communities. These tree buffers are known as “vegetative environmental buffers”, and they filter dust from the air before it is allowed to travel further downwind. However, there is limited knowledge on how effective buffers are at capturing dust, and current methods to measure effectiveness are unreliable. We used lidar (laser radar) to scan a dust plume downwind of a buffer. We found that the buffer captured between 21 and 74% of the dust that passed through it, depending on the time of day. It performed best at night and worst during the day.

TABLE OF CONTENTS

LIST OF TABLES

LIST OF FIGURES

LIST OF SYMBOLS

β	Backscatter coefficient
R	Distance from lidar along line of sight
B_0	Klett inversion scaling factor
α	Extinction coefficient
k	Klett inversion power constant
d_p	Equivalent sphere diameter
d_a	Aerodynamic equivalent diameter
ρ_w	Density of water
ρ_p	Particle density
κ	Dynamic shape factor
P	Relative backscatter power
α_{lidar}	Extinction coefficient obtained by the lidar
α_0	Assumed extinction coefficient
R_0	Range of assumed extinction coefficient
x	Axis parallel to VEB
y	Axis perpendicular to VEB
z	Vertical axis
α_{sample}	Expected total extinction of particulates in sampled volume of air
M	Total mass of particulates in sampled volume of air
m	Complex index of refraction of particles
λ	Laser wavelength
Q_{ext}	Mie extinction efficiency
$n(r)$	Number of particles of a given radius in sampled volume of air
C	Mass concentration
u	Wind speed perpendicular to VEB
v	Wind speed parallel to VEB
w	Vertical wind speed
U	Resultant horizontal wind speed
u_*	Friction velocity
K	von Karman constant
d_0	Displacement height
z_0	Aerodynamic roughness height
F	Mass flux
ER	Emission rate
m_e	Total mass emitted from VEB during run
m_r	Total mass released upwind of VEB during run
RR	Release rate
T	Total run time

LIST OF ACRONYMS

AFO	Animal feeding operation
VEB	Vegetative environmental buffer
PSD	Particulate size distribution
MEE	Mass extinction efficiency
LVTSP	Low-volume total suspended particulate
TKE	Turbulent kinetic energy

CHAPTER 1. BACKGROUND

Over the last few decades, advances in mechanical, biological, and chemical technologies have allowed for single farms to manage larger numbers of animals. As a result, every sector of animal husbandry has shifted toward large-scale production (MacDonald and McBride 2009). Large-scale production increases efficiency and reduces cost, but the practice concentrates animals onto smaller plots of land, concentrating animal-derived pollution. Pollution from animal agriculture is thus a growing concern. In particular, researchers and policy makers are focusing much attention on the measurement, modeling, control, and management of airborne emissions from agricultural sources (Aneja 2009). Concentrated animal feeding operations (CAFOs, or simply AFOs) emit particulate matter, ammonia, and several other constituents into the atmosphere in high concentrations, and the pollutants travel downwind while dispersing into neighboring communities, causing numerous community health and socioeconomic problems (Donham et al. 2007). In this study, we focused on the transport of particulate matter and its interaction with vegetative buffers, though our findings may implicate all pollutants emitted from AFOs.

Particulate matter, which consists of fecal matter, feed particles, and feather and epidermal fragments, is known to cause adverse health effects when inhaled (EPA 2009). In addition, it is well documented that particulates emitted from AFOs transport odorous compounds downwind (Burnett 1969; Hammond et al. 1979, 1981; Hammond and Smith, 1981; Yang et al. 2014). Odor creates a burden on communities and induces stress, and the complaint of odor is common amongst communities residing near AFOs (Wing et al. 2008; NRC 2003). Odor itself has been shown to cause adverse health effects, including eye, nose, and throat irritation, nausea, cough, shortness of breath, and alterations in mood (Schiffman 2000). A clear need exists to reduce particulate and associated odor emissions from AFOs. To serve this need, several post-emission mitigation strategies have been employed to absorb or deflect particulate emissions (Ni 2015). Vegetative environmental buffers (VEBs) are one technology commonly used.

Vegetative Environmental Buffers (VEBs, otherwise known as shelterbelts) are strategically placed rows of trees and shrubs that help control particulate emissions from

AFOs to the atmosphere. VEBs are highly regarded for their ability to: (1) enhance vertical mixing in the atmosphere, leading to dispersion and dilution; (2) filter particles mechanically by acting as a porous media; (3) precipitate particles by reducing wind speed; and (4) improve producer-community relations by providing a visual and noise barrier (Tyndall and Colletti 2007; USDA NRCS, 2007). In a recent survey in Iowa (Tyndall 2009), 52% of farmers reported currently using or expressed interest in using VEBs specifically to mitigate odor. With a growing demand for VEBs, it is critical that the understanding of the technology outpaces its application, so that extension services can be carried out adequately (Tyndall 2009).

At this point, our knowledge of VEB efficacy is lacking, and there is a need to quantify and document VEB performance. Due to the complex processes involved in a functioning VEB (1-4 described above), it is difficult to quantify VEB "performance". The VEB capture efficiency (percent of particulates retained by the VEB) is one simple measure of VEB efficacy. Capture efficiency measures only the effect of particulate trapping and neglects dispersion, dilution, and psychological effects. In this study, we conducted a field campaign to estimate VEB capture efficiency.

Estimating the VEB capture efficiency is difficult, because it requires emission rate measurements both upwind and downwind of a VEB. Conventional methods of measuring emission rates employ point sensors (Wang-Li 2013) to measure pollutant concentrations and flow rates. Sensors are placed at either an outlet point or some distance downwind of a facility. Emission rates (mass per time) are computed by multiplying concentration by flow velocity. When measuring at the outlet of a confined, tunnel-ventilated facility, this practice is straightforward (Li et al. 2013). However, in an open environment downwind of a VEB, it is more difficult to measure emission rates, since both concentrations and flow rates become significantly less uniform and more complex.

To compensate for the complexity, some researchers deploy arrays of time-integrating samplers over a large area. The sample points are often processed through spatial interpolation methods such as kriging (Carletti et al. 2000; Zirschky 1985), or by fitting a dispersion model (Jones et al. 2012; Faulkner et al. 2007). However, optimizing

sensor placement poses a challenge, and spatiotemporal geostatistical techniques for accurately placing monitors and interpolating measurements are lacking (Bunton et al. 2007). Furthermore, plumes emitted from animal production facilities have been shown to exhibit non-Gaussian dispersion and periodic lofting as a result of turbulence fields disrupted by the facilities themselves. In some cases, plumes reach up to 40 m above the ground surface, well above most sampling towers (Prueger et al. 2008; Holmén et al. 1998).

As a result of the complexities in estimating emission rates, few researchers have attempted to quantify VEB performance (Table 1). Wind tunnel studies (Laird 1997; Thernelius 1997) have proven useful for examining the entire plume extent to determine the capture efficiency in a laboratory setting. Field campaigns (Parker et al. 2012; Hernandez et al. 2012; Malone et al. 2006; Lin et al. 2006) have offered knowledge about a more realistic environment. However, these campaigns have used either point sensors or trained human panelists. Point measurements can only help quantify particulate or odor reduction between the specific locations where they are placed. An observed reduction in particulate count may be the result of the combined effects of dispersion, lofting, VEB capture, and a shift in the plume's trajectory. Therefore, experiments using point measurements have not estimated the total mass capture efficiency. Parker et al. (2012) recognized this deficiency and concluded that investigation into the differences between the various effects is warranted to fully understand VEB performance.

Table 1. Summary of past efforts to quantify the effectiveness of VEBs at reducing particulate matter and odor.

Reference	Reduction in Emissions	Methodology
Parker et al. 2012	66.3% reduction in odor at 15 m downwind	Trained human panelists; Sorbent tubes
Hernandez et al. 2012	40% reduction in total particulate counts; 40-60% reduction in odorous compound concentration	Optical particle counters; Sorbent tubes
Malone et al. 2006	49% reduction in particulate concentration	Gravimetric filters
Laird (1997) and Thernelius (1997)	35-56% reduction in particulate mass	Open-circuit wind tunnel, using digital imaging to relate brightness to dust deposition
Lin et al. 2006	68% reduction in odor 117m downwind	Trained human panelists

Lidar (light detection and ranging) has been used to obtain spatially-resolved estimates of particulate emission rates (Bingham et al. 2009; Lewandowski 2009). In this study, we adapted the lidar technique to estimate VEB particulate capture efficiency. The methodology presented herein addresses deficiencies in the existing techniques discussed above, and the results presented add to the lacking body of research documenting VEB capture efficiency.

CHAPTER 2. EXPERIMENTAL SITE & EQUIPMENT

2.1. Experimental Site

The study took place at the broiler house at the University of Delaware Carvel Research and Education Center (38.64, -75.47), between June 24 and 26, 2013. The multi-row VEB surrounding the facility was established in the Spring of 2003. In this study, we focused on the northeast section of the VEB and conducted experimental runs only when the wind was out of the southwest, perpendicular to the VEB. The northeast VEB section was planted 19 m from the exhaust fans in sequential rows parallel to the end wall of the broiler house with 12 bald cypresses (*Taxodium distichum*), 13 green giant arborvitaes (*Thuja plicata x standishii*), and 14 white pines (*Pinus strobus*). Each tree was 8 to 10 m tall. The closest row was 25 m from the northeast facility wall; rows were spaced 3 m apart, and all trees were planted 3 m apart. The dimensions of the VEB were 42 m x 12 m x 9 m (length x width x height) with an optical porosity of 0.18.

At the time of this study, the facility contained no chickens, and the exhaust fans were off. A surrogate particulate, kaolinite dust ($Al_2Si_2O_5(OH)_4$), was released at a known rate outside the facility and inside of the VEB. The dust was released continuously for six different runs, each ranging 3-6 hours in length, and each release was conducted at different distances from the inside edge of the VEB (Table 2). The lidar was positioned 410 meters northwest of the north edge of the VEB. Meteorological instruments and particulate size counters were arranged downwind of the VEB, where the lidar also scanned vertical slices in the atmosphere. A plan view of the study site (Figure 1, source: Google Maps), shows slices and the locations of the instruments deployed during this study.

Table 2. Summary of experimental runs.

Run	Date	Start Time (EDT)	Total Time (h)	Release Distance (m)
1	6/24/2013	10:52	2.95	5.2
2	6/24/2013	15:20	4.00	5.2
3	6/25/2013	8:48	4.00	9.1
4	6/25/2013	13:42	5.97	17.4
5	6/25/2013	20:23	3.42	9.1
6	6/26/2013	10:45	4.00	9.1

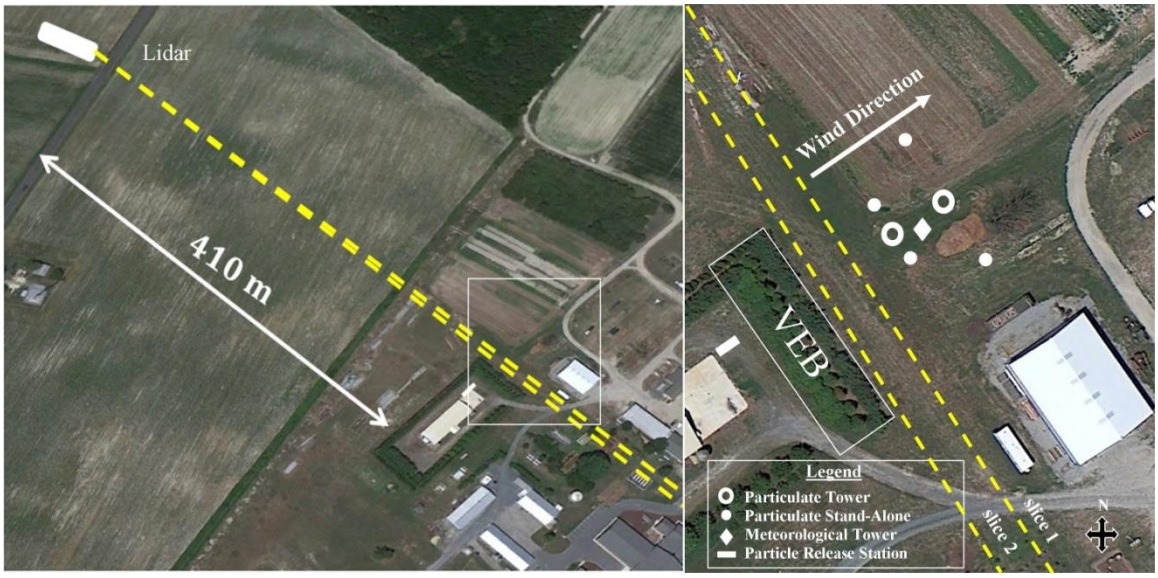

Figure 1. Aerial view of the study site. The lidar was positioned 410 m NW of the area of interest (left). Meteorological and particulate instruments were positioned downwind of the VEB, and the lidar scanned two slices immediately downwind of the VEB (right).

2.2. Lidar System

The University of Iowa's elastic scanning lidar (Figure 2) utilizes a laser, telescope, photo detector, and computer to measure the backscatter of light from suspended particulates. The lidar operates by emitting a pulse of infrared laser light (wavelength $\lambda = 1.064$ μm) into the atmosphere. Particulates interact with the pulse and scatter a fraction of the light back to the telescope. The scattering is elastic, so no energy is lost by the photons, and the detected light is at the same wavelength as the emitted light. The measured backscatter is related to the total extinction (backscatter + absorption) by a power law (Klett 1981; Klett 1985):

$$\beta(R) = B_0 \alpha^k(R), \quad (1)$$

where β is the backscatter coefficient, R is the distance from the lidar to a given sampling volume (m), B_0 is a scaling factor, α is the extinction coefficient (km^{-1}), and k is a power constant (assumed to be 1.0 in the lower atmosphere). The extinction coefficient is the variable of interest for lidar measurements. It is a measure of the energy lost in the beam per unit path length and is proportional to the particulate concentration. A detailed description of the specifications of the elastic lidar is shown in Table 3 and can be found in Kovalev and Eichinger (2004).

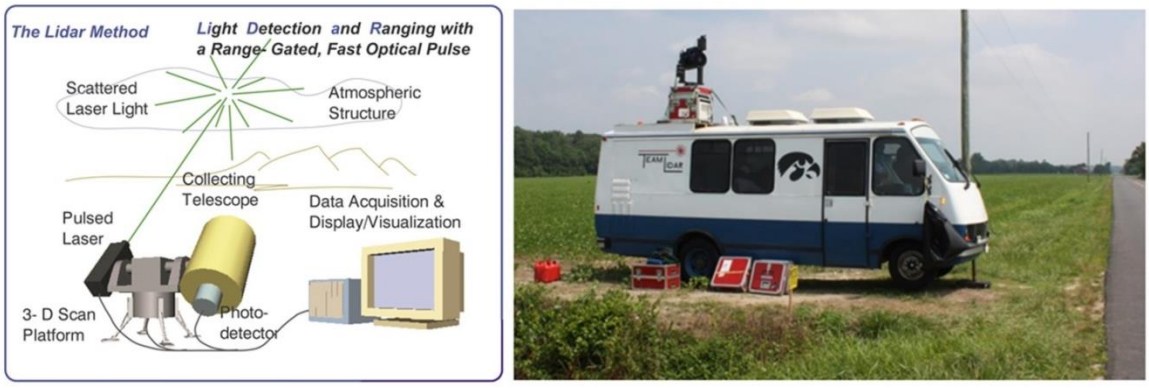

Figure 2. Left: The lidar works by emitting a pulse of light into the atmosphere, collecting backscattered light with a telescope, and ranging using the speed of light. Right: The University of Iowa elastic lidar was set up on a mobile research platform.

Table 3. Operating characteristics of the University of Iowa Scanning Miniature Lidar.

Transmitter		**Receiver**	
Wavelength	1064 nm	Type	Schmidt-Cassegrain
Pulse Length	~ 10 ns	Diameter	0.254 m
Pulse Repetition Rate	50 Hz	Focal Length	2.5 m
Pulse Energy	125 mJ max.	Filter Bandwith	3.0 nm
Beam Divergence	~ 3 mrad	Field of View	1.0 to 4.0 mrad adj.
		Range Resolution	1.5, 2.5, 5.0, 7.5 m
		Detector	IR-enhanced Silicon Avalanche Photo Diode

The lidar was used exclusively in the range-height indicator (RHI) scan mode. In this mode, the horizontal angle is fixed, and the lidar is stepped through a series of vertical angles. Stepping through vertical angles allows for the construction of a two-dimensional map of spatially-resolved extinction coefficients. The radial resolution of the measurements taken along each of the lidar beam lines of sight was ~1.5 m. The vertical angular resolution was 0.1 degrees, resulting in a vertical resolution between steps at the location of the plume of ~0.7 m. The horizontal angle was then changed to obtain another two-dimensional vertical slice slightly downwind of the first slice.

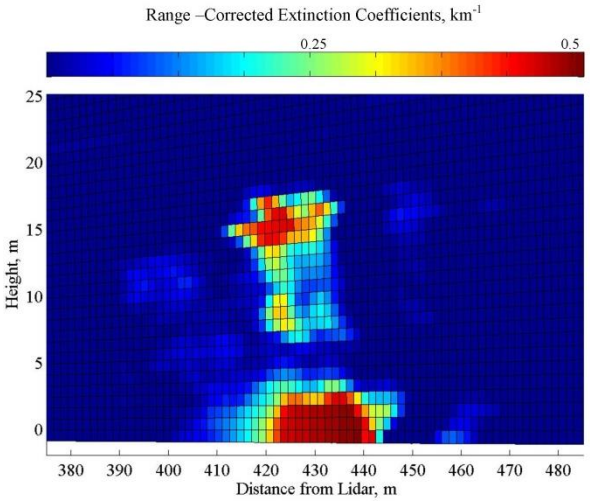

Figure 3. Range Height Indicator (RHI) scan. The VEB spans the ranges 410 - 460 m.

The lidar cycled between slice 1 and slice 2 continuously during each run. One scan required ~20 seconds to complete, and one cycle required ~1.3 minutes to complete. This acquisition technique resulted in 170-270 scans per slice for each run, depending on run duration. An example of a single RHI scan is shown in Figure 3.

Two slices taken immediately downwind of each other (6 m apart) offered redundancy in the estimate of capture efficiency. Assuming the 6 m strip of land between the two slices is an insignificant source/sink of particulates, the estimates from the two slices in a given run should approximate each other.

2.3. Meteorological Instruments

Meteorological measurements were obtained from instruments mounted on a 10-m tower placed 29 m downwind of the VEB (Figure 4). The tower was instrumented with three Campbell Scientific (Logan, UT) CSAT3 3D high frequency sonic anemometers situated at 2.3, 5.0, and 8.9 m above the surface; three Vaisala (Vantaa, Finland) HMP 45C temperature and humidity probes at 2.3, 5.0, and 8.9 m above surface; and one LiCor (Lincoln, NE) 7500 Infrared Gas Analyzer (CO_2 and water vapor) at 2.3 m above the surface. The meteorological instruments were powered by deep cycle marine batteries connected to solar panels. All high frequency instruments (sonic and IRGA) were sampled at 20 Hz while temperature and humidity data (low frequency instruments) were sampled at 10-second intervals and output as 10-minute averages.

Figure 4.Meteorological tower, with sonic anemometer and IRGA (left) and temperature & humidity probe (bottom right).

.

2.4. Particulate Release Station

A particle release station, which consisted of a fan, a discharge tunnel, and particulate releasing unit (Figure 5), allowed for the controlled release of particulates. The 2.4 m long discharge tunnel was made of foam insulation boards and attached to the inlet side of a 0.9-m diameter box fan (Model: MF-36P-D-S, Cumberland, Assumption, IL) with a 1.0 m x 1.0 m opening. The fan and tunnel were placed at the ground level with an airflow rate of 17,700 m^3/h. The releasing unit upwind of the discharge tunnel included a wrist action shaker (Model: BB, Burrell, Pittsburgh, PA), two mini sprayers (Model: BAD260-3, Badger Air-Brush Co., Franklin Park, IL), an air pressure regulator, and an air compressor. The two sprayers were mounted side-by-side 0.4-m above the ground surface on the shaker upside down and shaken at a rate such that the particles did not settle. Air pressure was maintained at 41,400 Pa (6 psi). The containers of the two sprayers were filled with kaolinite fine particles and weighed before and after each release. The particles in each container were released at a controlled rate in the range of 10.0 to 14.0 g/min and were depleted in about 7 to 10 min.

Figure 5. Particulate release station.

2.5. Particulate Samplers

Particulate size distributions (PSD) were obtained from samplers mounted on two 10-m tall towers and from six stand-alone sampler units. The samplers were positioned downwind of the release point and arranged in an array, as displayed in Figure 1. Each tower held three low-volume (target flow rate = 16.7 liters per minute, lpm) total suspended particulate (LVTSP) sampler heads designed by Texas A&M/USDA-ARS (Wanjura et al. 2005), which were located at 4.5, 7.25, and 10 m above the surface. Each stand-alone unit held one LVTSP sampler head positioned at 1.5 m above the surface.

CHAPTER 3. DATA ANALYSIS METHODS

In this section, the technique is presented for inverting lidar, wind, and particulate size data into capture efficiency. The analysis presented below was performed for all six runs. Each variable needed to calculate capture efficiency was time-averaged over the run duration, yielding six total estimates. In the methodology described hereafter, overbars ($\bar{}$) indicate time-averaging over the run duration.

3.1. Particulate Size Distribution

Particulate size distributions (PSDs) were required to obtain mass extinction efficiency, a parameter needed to invert extinction coefficients to mass concentration. PSD methods are described in Wang-Li et al. (2013) and Buser (2004); a brief summary of the method is provided here. A Beckman Coulter LS230 laser diffraction system (Beckman Coulter Inc., Miami, FL) with software version 3.29 was used to perform the particle size analyses on the filter and wash samples. The instrument sizes particles with diameters ranging from 0.4 to 2,000 µm. The LS230 fluid module was used with a 5% lithium chloride/methanol suspension fluid mixture that had a fluid refractive index of 1.326. Approximately 10-L batches of the suspension fluid were prepared and stored in a self-contained, recirculating filtration system equipped with 0.2 µm filters to keep the fluid well mixed and free of larger particles. Prior to each test run, a background particle check was performed on the fluid to help minimize particulate contamination from non-sample sources.

The optical model used in calculating the PSD was based on real and imaginary refractive indices of 1.56 and 0.01, respectively, for each sample. These refractive index values are typical for quartz, clay minerals, silica, and feldspars (Buurman et al. 2001). The LS230 PSD results were in the form of particle volume versus equivalent spherical diameter, denoted as d_p (µm): and were converted to particle volume versus aerodynamic equivalent diameter, denoted as d_a (µm):

$$d_a = d_p\left(\frac{\rho_p}{\kappa\rho_w}\right), \tag{2}$$

where ρ_w is the density of water with a value of 1 g cm^{-3}, ρ_p is the particle density (g cm^{-3}), and κ is the dynamic shape factor (dimensionless). The kaolinite dust density was determined to be 2.8 g cm^{-3}, consistent with the supplier's specification.

3.2. Lidar Signal Inversion

The Klett method (Klett 1981; Klett 1985; Krichbaumer and Werner 1994; Kovalev and Eichinger 2004) was used to invert the relative backscatter power $P(R)$, measured by the lidar, to extinction coefficients at various ranges from the lidar $\alpha_{lidar}(R)$ (km^{-1}):

$$\alpha_{lidar}(R) = \frac{P(R)R^2}{\frac{P(R_0)R_0^2}{\alpha_0} + 2\int_R^{R_0} P(R')R'^2\, dR'}, \tag{3}$$

where $\alpha_0 = \alpha(R_0)$ is an assumed extinction coefficient at a range R_0. Using the lidar in scanning mode allowed range resolved extinction coefficients $\alpha_{lidar}(R)$ to be transformed into two-dimensionally spatially resolved extinction coefficients $\alpha_{lidar}(x,z)$.

A relationship is needed between the measured light extinction and mass concentration in order to determine emission rates. This relationship is known as the Mass Extinction Efficiency (MEE, m^2 g^{-1}) (Husar and Falke 1996; Lagosas et al. 2005):

$$MEE = \frac{\alpha_{sample}}{M}, \tag{4}$$

where α_{sample} (m^{-1}) is the expected total fraction of light attenuated per unit path length by the all the particulates sampled in a volume of air, and M (g m^{-3}) is the total mass of the particulates sampled in a volume of air. α_{sample} and M are determined by using the PSDs measured by the LVTSPs.

Mie scattering theory describes the scattering of light by a homogeneous sphere with a diameter comparable to the wavelength of incident light. Knowing the refractive index of the particles (m = 1.56 +0.01i) and laser beam wavelength λ, one can calculate the Mie extinction efficiency, Q_{ext} (dimensionless), for all particle sizes sampled (Bohren

and Huffman 1983). The Mie extinction efficiency is the ratio of the extinction coefficient to the cross-sectional area of the particle:

$$Q_{ext} = \frac{\alpha_{sample}}{\pi \cdot r^2}, \tag{5}$$

where r is the radius of the particle (m). Rearranging Equation (5), the product of the particle cross-sectional area and the Mie extinction efficiency for each of the particles integrated over the entire size spectrum results in the inferred particulate extinction coefficient expressed as:

$$\overline{\alpha}_{sample} = \pi \int_{r_1}^{r_2} r^2 Q_{ext}(r, \lambda, m) \overline{n}(r) dr, \tag{6}$$

where $\overline{n}(r)$ (m^{-3}) is the number of particles of a given particle radius in the sampled volume of air and represents the PSD averaged over the run duration. Knowing the PSD and particle density ρ_p, the mass of the sampled air is easily calculated:

$$\overline{M} = \frac{4}{3} \pi \rho_p \int_{r_1}^{r_2} r^3 \overline{n}(r) dr. \tag{7}$$

Therefore,

$$\overline{MEE} = \frac{\overline{\alpha}_{sample}}{\overline{M}} = \frac{\pi \int_{r_1}^{r_2} r^2 Q_{ext}(r, \lambda, m) \overline{n}(r) dr}{\frac{4}{3} \pi \rho_p \int_{r_1}^{r_2} r^3 \overline{n}(r) dr}. \tag{8}$$

Equation (8) links the extinction coefficient to the particulate mass concentration. Averaging all the lidar scans obtained within the run duration $\overline{\alpha}_{lidar}(x, z)$ and applying the above relation, the average two-dimensional spatially-resolved particulate mass concentration $\overline{C}(x, z)$ (mg m^{-3}) is determined:

$$\overline{C}(x, z) = \frac{\overline{\alpha}_{lidar}(x, z)}{\overline{MEE}}. \tag{9}$$

3.3. Wind Profile Modeling

To calculate the emission rate through the VEB, the mean wind speed perpendicular to the VEB ($\bar{u}$) was required at all *(x,z)* for which mass concentration was known. Wind speed was only measured at three points, so some wind speed modeling was implemented. The wind speed profile was first assumed horizontally homogeneous and therefore a function of height alone. For heights below the highest anemometer (8.9 m), $\bar{u}$ was linearly interpolated between the three sonic anemometer measurements, with zero wind speed assumed at the surface. For heights above 8.9 m, Similarity Theory (Monin and Obukhov 1954) was used to estimate the wind speeds at the corresponding lidar scan heights:

$$\overline{U}(z) = \frac{\bar{u}_*}{K} \cdot \ln\left(\frac{z - d_0}{\bar{z}_0}\right), \tag{10}$$

where $\overline{U}$ is the resultant horizontal wind speed (computed from u and v velocity components) (m s^{-1}), $\bar{u}_*$ is the friction velocity (m s^{-1}), K is von Karman's constant 0.40 (dimensionless), d_0 is the displacement height (m), and $\bar{z}_0$ is the aerodynamic roughness height (m). The friction velocity is the surface momentum flux expressed in terms of velocity units and is defined by:

$$\bar{u}_* = \overline{\left(\left(\overline{u'w'}\right)^2 + \left(\overline{v'w'}\right)^2\right)^{1/4}}, \tag{11}$$

where u, v, and w are the 3 components of the wind velocity (m s^{-1}); primes denote deviations about the 10-minute mean of the velocity components, and overbars denote 10-minute mean values. d_0 was assumed to be 64% of the tree height (9 m), or 5.8 m (Cowan 1968; Stanhill 1969). $\bar{z}_0$ was calculated empirically by rearranging Equation (10) to solve for $\bar{z}_0$ at the highest anemometer.

The parameters ($\bar{u}_*$ and $\bar{z}_0$) in Equation (10) are based on the resultant horizontal wind speed. In order to model the perpendicular wind profile $\bar{u}(z)$, a correction for wind direction was needed:

$$\bar{u}(z) = \bar{U}(z) \cdot \frac{\bar{u}_{8.9}}{\sqrt{\bar{u}_{8.9}^{-2} + \bar{v}_{8.9}^{-2}}}, \tag{12}$$

where the subscripts indicate that the correction is performed at the highest anemometer, 8.9 m above the ground surface. For each run, a unique wind profile was constructed. Figure 6 contains an example of the perpendicular wind profile for run 6.

3.4. Emission Rate and Capture Efficiency

Mass concentrations were multiplied by the perpendicular wind speeds to obtain mass fluxes $\bar{F}(x,z)$ (mg m^{-2} s^{-1}) through the measured plane:

$$\bar{F}(x,z) = \bar{C}(x,z) \cdot \bar{u}(z). \tag{13}$$

Flux estimations were multiplied by the area in the (x,z) plane of each sample volume and then summed in order to obtain emission rates $\overline{ER}$ (mg s^{-1}) :

$$\overline{ER} = \sum_{x=375}^{x=485} \sum_{z=0}^{z=40} \bar{F}(x,z) \cdot \Delta x \cdot \Delta z. \tag{14}$$

The area of interest, as expressed in Equation (14), was between 375 and 485 m from the lidar and between 0 and 40 m above the surface. VEB efficiency was defined as:

$$\textit{Capture Efficiency} = \left(1 - \frac{m_e}{m_r}\right) \cdot 100\% = \left(1 - \frac{\overline{ER} \cdot \Delta t}{\int_0^T RR \cdot dt}\right), \tag{15}$$

where m_e is the total mass emitted from the VEB during the run (g), m_r is the total mass released upwind of the VEB during the run, RR is the release rate upwind of the VEB (mg s^{-1}), and T is the total run time (s). A summary of the method is shown in Figure 6.

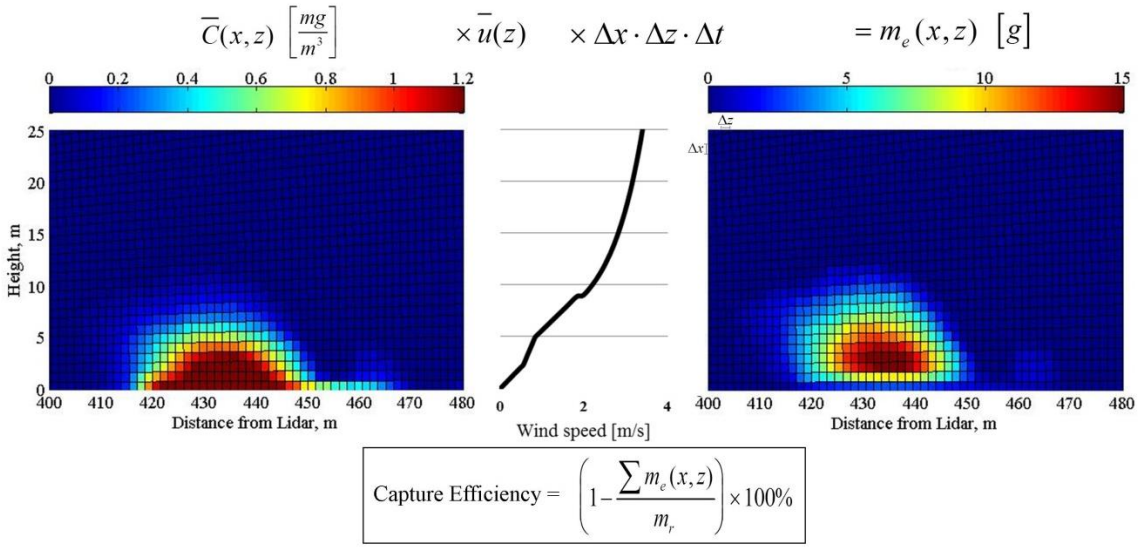

Figure 6. Visualization of method for determining capture efficiency. Spatially-resolved concentrations (left) are multiplied by the perpendicular wind speed profile (middle), cross sectional areas, and total run time to obtain a spatially-resolved map of the total mass emitted from the VEB (right). The masses are integrated over the spatial domain and compared with the total mass released to determine capture efficiency (bottom).

CHAPTER 4. UNCERTAINTY ANALYSIS

4.1. Lidar Signal Inversion Uncertainty

The uncertainty in the transformation of the raw lidar signal into extinction coefficients propagates to the capture efficiency estimation. Klett's Lidar inversion algorithm (Equation (3), rewritten below for reference) contains 4 major sources of uncertainty which propagate to the extinction coefficient $\alpha(R)$.

$$\alpha_{lidar}(R) = \frac{P(R)R^2}{\frac{P(R_0)R_0^2}{\alpha_0} + 2\int_R^{R_0} P(R')R'^2\, dR'}, \tag{3}$$

The first source is the average fractional uncertainty of the range corrected lidar measurement, $P(R)R^2$ in the numerator. This uncertainty is related to the signal to noise ratio of the system and is evaluated at the average range, R_{AVG} which in this case is about 440m. The nature of the R^2 correction to the lidar measurements implies that this uncertainty tends to be smaller closer to the lidar and greater further away from the lidar. The root mean square noise level is less than 10 mV out of approximately 900 mV at a range of 440 m, with closer ranges having less uncertainty and longer ranges having more. The uncertainty from this source is estimated on average at 1% for this application.

$$\frac{\delta\alpha_1}{\alpha} = \frac{\delta P(R)R^2}{P(R_{AVG})R_{AVG}^2} \approx 1\%. \tag{16}$$

The second source of uncertainty in the lidar inversion is related to the uncertainty of the integral in the denominator of Equation (3), which is a function of how many lidar measurements are summed. For a clear atmosphere, the integral in the denominator in Equation (3) usually does not dominate the first term in the denominator, but is comparable in magnitude. For simplicity of the estimate, we assume the magnitude of the two terms in the denominator are approximately equal, that

$$\frac{P(R_0)R_0^2}{\alpha_0} \approx \int_{R_0}^{R} P(R_0')R_0^{2\prime}\, dR'.$$

If we assume that the errors in each of the lidar values are statistically independent, then the uncertainty is related to the number of data samples, *N*, used for the integration which was well over 150 for this study. The uncertainty associated with this source is estimated at about 4%.

$$\frac{\delta\alpha_2}{\alpha} = \frac{\delta\left(\int_{R_0}^{R} P(R')R^{2}\,'dR'\right)}{\frac{P(R_0)R_0^2}{\alpha_0} + \int_{R_0}^{R} P(R')R^{2}\,'dR'} \approx \frac{\sqrt{N}}{2N} = 4\%\,. \tag{17}$$

The third source of uncertainty in the inversion is linked to the value of the known extinction coefficient, α_0, at the distance R_0. In this study, we have assumed that the atmosphere is relatively clean in areas far from the facility, so that the assumed extinction is mostly molecular. This assumption is checked by examining the extinction coefficients before and after the plume. These extinction coefficients should be approximately the same; if they are not, the initial estimate was in error. We estimate the uncertainty of the assumption of α_0 at 5%. Again we note that the two terms in the denominator are of comparable size. This leads to an overall uncertainty in the extracted extinction coefficient of about 2.5%.

$$\frac{\delta\alpha_3}{\alpha} = \frac{\frac{\delta\alpha_0}{\alpha_0}\left(\frac{P(R_0)R_0^2}{\alpha_0}\right)}{\frac{P(R_0)R_0^2}{\alpha_0} + \int_{R_0}^{R} P(R')R^{2}\,'dR'} \approx \frac{1}{2}\frac{\delta\alpha_0}{\alpha_0} = 2.5\%\,. \tag{18}$$

The fourth lidar inversion related source is the uncertainty of the actual value of the range corrected lidar signal at the location of the estimated extinction, α_0 which is $P(R_0)R_0^2$. The uncertainty of the signal in far range is estimated to be 5%, which results in a 2.5% contribution in the extracted extinction coefficients.

$$\frac{\delta\alpha_4}{\alpha} = \frac{\frac{\delta P(R_0)R_0^2}{\alpha_0}}{\frac{P(R_0)R_0^2}{\alpha_0} + \int_{R_0}^{R} P(R')R^{2}\,'dR'} \approx \frac{1}{2}\frac{\delta P(R_0)R_0^2}{P(R_0)R_0^2} = 2.5\%\,. \tag{19}$$

Combining the above inversion uncertainties in quadrature results in 4% overall uncertainty (assuming the independence of the sources of error). This value is unusually small and is due to the particular conditions in this problem. Most of the contributing data was located near the VEB and close to the lidar where the accuracy and repeatability of the measurement is high and allows a higher quality estimate of the far range extinction coefficient α_0.

$$\frac{\delta\alpha_{LIDAR}}{\alpha} = \sqrt{\left(\frac{\delta\alpha_1}{\alpha}\right)^2 + \left(\frac{\delta\alpha_2}{\alpha}\right)^2 + \left(\frac{\delta\alpha_3}{\alpha}\right)^2 + \left(\frac{\delta\alpha_4}{\alpha}\right)^2} \approx 4\% \qquad (20)$$

4.2. Mass Extinction Efficiency Uncertainty

The uncertainty in the PSD measurements correspond to uncertainty in MEE values and propagate to capture efficiency estimates. The uncertainty in MEE is represented by the standard deviation of the MEE values estimated at all sampler locations. For example, in run 6, a total of 12 size distributions were measured. MEE values calculated from these distributions ranged from 0.309 to 0.338, with an average of 0.322 and standard deviation of 0.0093 for a fractional error of 3%. The MEEs calculated at various locations for a given run are remarkably consistent. Because MEE is a ratio of two averages, changes in PSD must be significant to change the MEE appreciably.

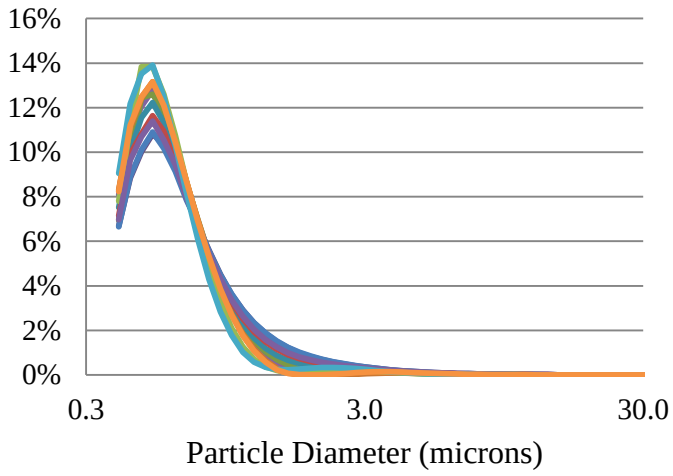

Figure 7. PSDs at various locations for run 6.

Another source of the uncertainty was the assumption of the particle density (assumed to be 2.80 g cm^{-3} for this analysis). While the literature reports up to 70% spread in the values of the biogenic particle density from a widely accepted average value of 1 g cm^{-3} (Murphy et al. 2004; Wang and Walter 1987), the kaolinite dust used here is well characterized. The uncertainty associated with the density of the released

particulates was chosen to be of order 2%. The overall uncertainty associated with MEE estimates was 4%.

4.3. Wind Analysis Uncertainty

We distinguish two sources of error related to the wind speed estimates. The first error contribution comes from the modeled vertical wind profile, and the second comes from the difference in the wind profile at the location of the measurements and the wind profile at the location of the lidar scans. There is no established method to determine the uncertainty of a modeled wind profile. The uncertainty is assumed to be 10%. This estimate is likely high, as the wind velocity was measured at three heights. However, large turbulent structures and non-logarithmic vertical profiles are often generated near a VEB, so this estimate represents the complexity associated with vertical profiles in close proximity to a VEB.

To assess the uncertainty associated with the wind profile measurement location, the differences in the estimates of capture efficiency between slices 1 and 2 are examined. We conservatively attribute all differences in capture efficiencies between slices 1 and 2 in a given run to the change in the wind profile between the two slices and the measured wind profile. Fractional differences in capture efficiency between slices 1 and 2 averaged 17%.

4.4. Capture Efficiency Uncertainty

Combining the lidar, MEE, and the wind analysis uncertainty, the overall uncertainty of the emission rates estimate from this study is given by:

$$\frac{\delta(\mathrm{ER})}{\mathrm{ER}} = \sqrt{\left(\frac{\delta\alpha_{LIDAR}}{\delta\alpha_{LIDAR}}\right)^2 + \left(\frac{\delta MEE}{MEE}\right)^2 + \left(\frac{\delta\rho_{PARTICLE}}{\rho_{PARTICLE}}\right)^2 + \left(\frac{\delta u_{PROFILE}}{u_{PROFILE}}\right)^2 + \left(\frac{\delta u_{LOCATION}}{u_{LOCATION}}\right)^2}$$

$$= \sqrt{(0.04)^2 + (0.03)^2 + (0.04)^2 + (0.10)^2 + (0.17)^2} \cong 0.203 = 20\% \qquad (21)$$

CHAPTER 5. RESULTS & DISCUSSION

5.1. Observed VEB Capture Efficiencies

The capture efficiencies ranged between 21 and 74% amongst the six runs (Table 4). The performance of the VEB varied based on time of day. The VEB captured a larger fraction of particulates during the night and a smaller fraction during the day (Figure 8). Five of the six runs were performed during the day, one at night. Since sampling times were non-uniformly distributed amongst a 24-hour period, the average diurnal capture efficiency was not determined. It is more appropriate to report the range of 21 to 74% based on this data. A wide range of capture efficiency illustrates the complex dynamics associated with VEBs.

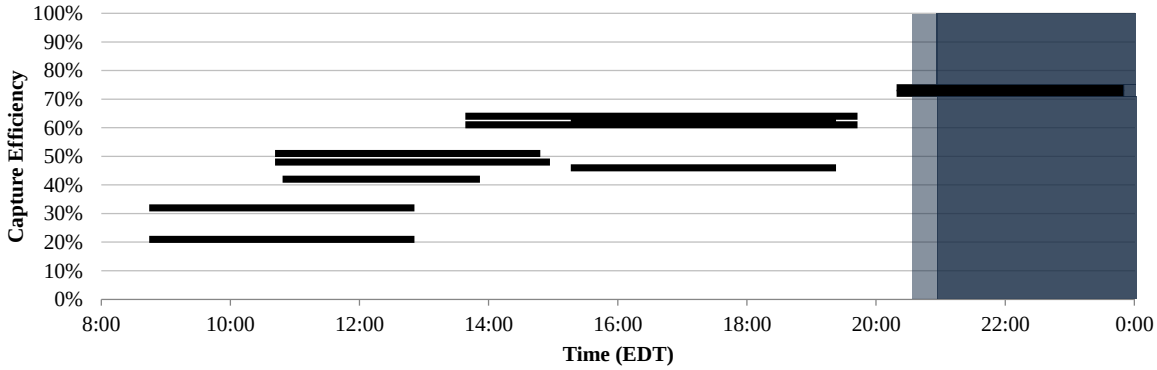

Figure 8. Capture efficiency vs. time of day. Capture efficiencies measured over the three day span are combined into one timeline. Shading indicates night time.

5.2. Factors Influencing Capture Efficiency

Several variables influenced the capture efficiency, including the wind speed and direction, turbulence intensity, and release position. All of these variables changed between and during runs. With only six observations and no single variable held constant, it was difficult to precisely quantify the influence of each variable on capture efficiency. However, some general tendencies were observed.

5.2.1. Turbulent Kinetic Energy

Turbulence has been shown to dominate transport from AFOs to the surrounding atmosphere (Prueger et al. 2008), and it is likely that turbulence contributed to the VEB performance. Turbulent kinetic energy (TKE) is a measure of the energy embedded in the turbulent component of the wind per unit air density ($m^2\ s^{-2}$):

$$\text{TKE} = \frac{1}{2}\left(\overline{u'^2} + \overline{v'^2} + \overline{w'^2}\right), \tag{22}$$

where *u*,*v*, and *w* are the wind velocity components, overbars denote mean values, and primes denote fluctuations about the mean values. TKE within the VEB is primarily produced mechanically, and mechanical production is augmented by buoyant processes. As the mean wind advects over the facility, it encounters bluff-body obstacles. A range of shear forces develop, and three-dimensional turbulent eddies result. Surface fluxes (sensible and latent heat) also contribute to TKE production. Daytime surface heating creates density inversions in the surface layer, and vertical motion results, enhancing TKE production within the VEB. Conversely, nighttime surface cooling generates a stably stratified layer which degrades TKE.

This experiment was performed within the roughness elements (the buildings and trees) of the atmospheric surface layer, where mechanical generation of TKE is expected to dominate; there is experimental evidence that supports this expectation. Mechanical TKE production is highest during windy time periods, as greater shear forces develop from larger velocity gradients near the surface. Buoyant production depends on the surface sensible and latent heat fluxes significantly more than the wind speed. Therefore, in a mechanically dominated regime, a strong relationship between TKE magnitude and wind speed should exist, and the spread should be minimal. Indeed, this experiment demonstrated such a relationship (Figure 9).

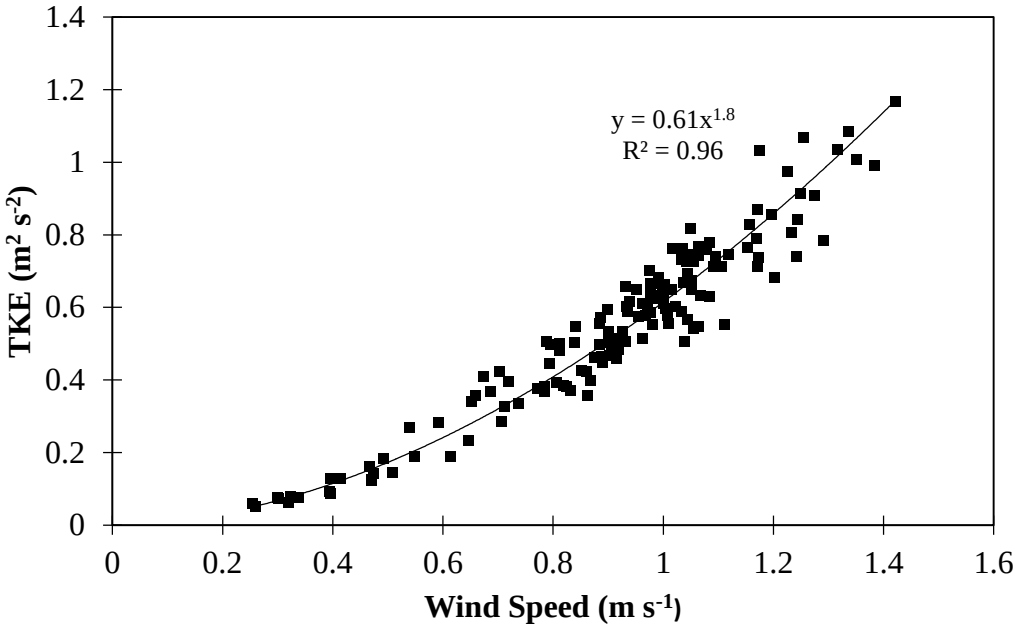

Figure 9. Turbulent kinetic energy and wind speed observed during the experimental runs at 2.3 m above the surface.

During the daytime runs, the atmosphere within the VEB remained slightly unstable, with the Monin-Obukhov stability parameter (z/L) ranging from -0.12 to -0.02. Similarly, the atmosphere was slightly stable during the nighttime run, with a z/L of +0.17. The observed range of -0.12 to 0.17 z/L represents a near-neutral atmosphere, during which mechanical production of TKE dominates over buoyant production. Still, a slightly negative z/L indicates that surface fluxes are positive, which has some mixing effect. A slightly positive z/L indicates negative surface fluxes, and mixing is suppressed to some degree. In summary, we characterize the turbulence within the VEB as mechanically-dominated and enhanced or suppressed by buoyancy.

Table 4. Experimental results.

Run	Start Time (EDT)	Total Time (h)	Release Distance (m)	z/L	TKE (m^2s^{-2})	Capture Efficiency Sl.1	Sl.2
1	10:52	2.95	5.2	-0.12	1.3	42%	—
2	15:20	4.00	5.2	-0.02	1.8	62%	46%
3	8:48	4.00	9.1	-0.10	1.6	32%	21%
4	13:42	5.97	17.4	-0.05	1.9	64%	61%
5	20:23	3.42	9.1	0.17	0.32	74%	72%
6	10:45	4.00	9.1	-0.12	1.4	51%	48%

The VEB least effectively removed particulates during the daytime runs (capture efficiency = 47 ± 14 %, n = 9), when TKE was relatively high—ranging from 1.3 - 1.9 $m^2 s^{-2}$ at 9 m above the surface. The VEB was most effective during the nighttime run (capture efficiency = 73 ± 1.5 %, n = 2), when TKE was relatively low (0.32 $m^2 s^{-2}$). The VEB therefore performed best during times with lesser turbulence. Since the wind speed was well-correlated with TKE, the VEB also performed best during times of slower wind speeds.

5.2.2. Periodic Lofting

Turbulence may have contributed to periodic lofting. A series of scans is presented in Figure 10, where plumes are shown to rise well above the 9 m tall VEB. During these events, there is no interaction between the plume and VEB, and none of the lofted particulates are captured. Periodic lofting is therefore an undesirable process from the perspective of capturing particulates. However, periodic lofting can enhance dilution and reduce odor concentrations downwind of the source. Thus a trade-off exists between particulate capture and lofting/dispersion. While this study has presented a range of capture efficiencies, future research may help realize the optimum proportion of capture vs lofting processes. Further, knowledge of these proportions will help engineer future VEBs.

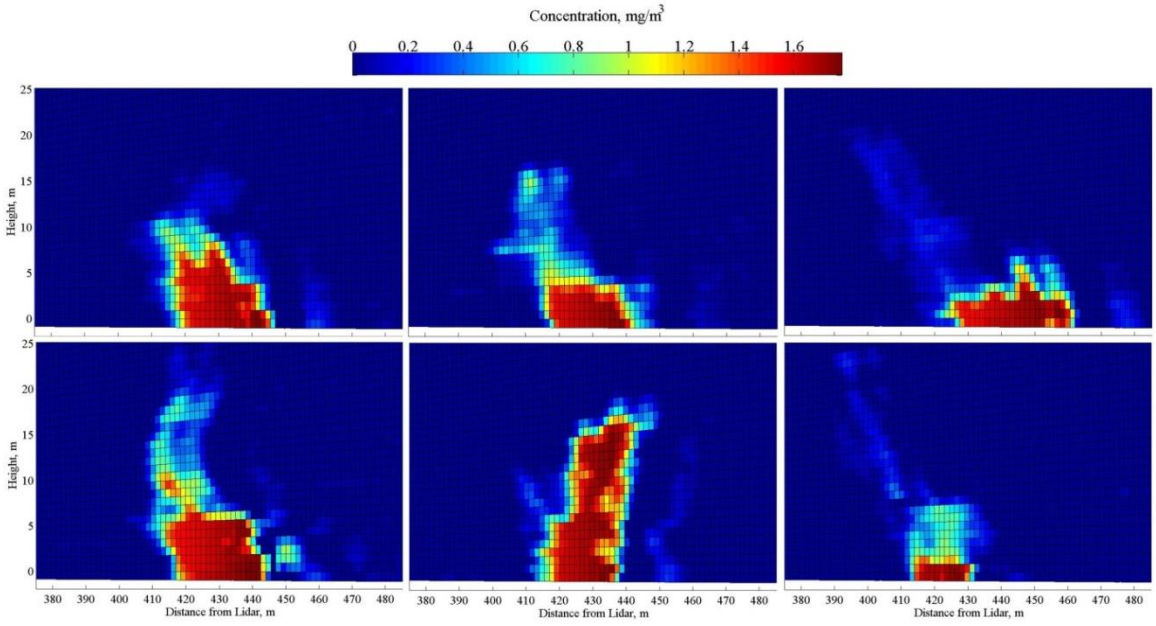

Figure 10. Progression of vertical lidar scans for run 6. The VEB spans the ranges 410 – 460 m from the lidar, and the wind is blowing orthogonal to the surface, into the page.

5.2.3. Release Distance

VEB design considerations include height, thickness, porosity, tree species, and orientation. Research investigating the effect of each of these variables on capture efficiency is limited. In this study, we varied the release distance from the VEB in an effort to determine a recommended distance VEBs should be built from the facility. Due to the varying nature of atmospheric conditions throughout the day, it is appropriate to contrast results obtained at the same time of day under similar atmospheric conditions. Runs 1 and 6 and runs 2 and 4 are examined. The VEB captured 8% more particulate mass in run 6 (9.1 m release distance) than in run 1 (5.2 m release distance). It captured 9% more particulate mass in run 4 (17.4 m release distance) than in run 2 (5.2 m release distance). In both cases, a further distance between the discharge tunnel and the buffer resulted in a higher VEB capture efficiency under the same atmospheric conditions. However, these results are not complete and should be considered preliminary.

5.3. Plume Structure

During each run, between 170-270 lidar scans were collected for each slice. Typical scans are shown in Figure 10. The scans taken throughout this campaign clearly show small individual plume structures intermittently lofting high into the atmosphere, well above the VEB or any ground-based measurement height. These observations are consistent with those reported in Prueger et al. (2008) and Holmén et al. (1998), and they justify the use of lidar to measure the entire plume. However, when scans are averaged over a run duration, they appear Gaussian (see Appendix). These unexpected results have implications in emissions monitoring and future quantification of VEB performance. It seems that given an adequate averaging time, plumes emitted from VEBs converge to a Gaussian shape. With this information, future researchers can deploy arrays of point measurements immediately downwind of VEBs and use inverse Gaussian modeling to determine emission rates.

However, significant questions remain. To the best of our knowledge, this is the first attempt at averaging many lidar scans downwind of an AFO over a few hours. The first question is whether a Gaussian plume results from the presence of a VEB in the flow field, or if it is characteristic of all AFOs. To address this question, a lidar campaign

could be conducted similar to this study, but in the absence of a VEB. The second question is what averaging period is adequate for Gaussian plumes to emerge. The answer to this question will guide future researchers and policy makers in conducting monitoring studies and setting emission guidelines. Finally, open feedlots still contribute a significant fraction of animal production. The Gaussian plumes observed in this study were the result of a tunnel-ventilated, point source facility, and open feedlots act as area sources. Extended sources can be expected to be considerably more complex.

5.2. Comments on the Measurement Technique

This paper outlines methodology to estimate spatially-resolved particulate concentrations and emission rates using lidar and applies these estimates to determine VEB capture efficiency. The VEB exhibited a wide range of efficacy, capturing 21-74% of particulate mass. The observed capture efficiencies compare with the reported range of 35-68% in the existing literature (Table 1). This agreement provides confidence that the lidar technique for estimating emission rates is effective, at least to first order.

The lidar technique provides reliable estimations of emission rate with an uncertainty of 20%. As the wind speed uncertainty contributes the most to the overall uncertainty, the use of spatially resolved wind profile measurements would significantly improve the accuracy of the estimate. In addition to estimating the capture efficiency, the lidar technique can effectively estimate plume transport further downwind of the source, when crosswinds and lofting make it difficult to obtain point measurements. We note that this method can also be applied to the estimation of emissions of any chemical species given a lidar capable of measuring that species.

CONCLUSIONS

The methodology presented here is a reliable technique for estimating emission rates under complex flow regimes. The method was applied to determine the capture efficiency of a VEB, as documentation of VEB efficacy is currently lacking.

The results of this study indicate that a VEB can effectively capture between 21 and 74% of PM transported through it, depending on atmospheric conditions. Higher capture efficiency is observed at night, during stable atmospheric conditions with low TKE. However, the same conditions may discourage lofting and consequently result in more odor nuisance to downwind neighbors. Conditions associated with low capture efficiency (daytime, unstable, and high TKE) may encourage lofting and dispersion.

Capture efficiencies exhibited a slight relationship with the particulate release distance from the VEB. Due to the limited number of runs performed and the varying atmospheric conditions associated with each run, only two pairs of runs were available with similar atmospheric conditions and different release distances. Under both situations, a further release distance yielded greater capture efficiencies.

The results of this experiment show that a VEB is an effective mitigation strategy for capturing particulate matter which often transports malodorous compounds. Even during its worst performance, the VEB captured 21 % of particulates, and at its best, it captured 74 %. We hope these results will provide farmers with some assurance that the technology many of them are interested in implementing (or have already implemented) is in fact effective.

REFERENCES

Aneja, V. P., W. H. Schlesinger, and J. W. Erisman, 2009: Effects of agriculture upon the air quality and climate: Research, policy, and regulations. *Environ. Sci. Technol.,* **43**, 4234-4240, doi: 10.1021/es8024403.

Bingham, G. E., and Coauthors, 2009: Lidar based emissions measurement at the whole facility scale: Method and error analysis. *J. Appl. Remote Sens.,* **3**, 033510, doi: 10.1117/1.3097919.

Bohren, C.F., nad D.R. Huffman, 1983: *Absorption and Scattering of Light by Small Particles.* John Wiley & Sons, 530 pp.

Bunton, B., and Coauthors, 2007: Monitoring and modeling of emissions from concentrated animal feeding operations: overview of methods. *Environ. Health Perspect.,* **115** 303-307.

Burnett, W. E., 1969: Odor transport by particulate matter in high density poultry houses. *Poult. Sci.,* **48**, 182-185.

Buser, M.D., 2004: Errors associated with particulate matter measurements on rural sources: appropriate basis for regulating cotton gins. Diss., Texas A&M University, 348 pp.

Buurman, P., Th. Pape, J.A. Reijneveld, F. de Jong, and E. van Gelder, 2001: Laser-diffraction and pipette-method grain sizing of Dutch sediments: correlations for fine fractions of marine, fluvial, and loess samples. *Geol. Mijnbouw,* **80**, 49-57.

Carletti, R., M. Picci, and D. Romano, 2000: Kriging and bilinear methods for estimating spatial pattern of atmospheric pollutants. *Environ. Monit. Assess.*, **63**, 341-359.

Cowan, I. R, 1968: Mass, heat and momentum exchange between stands of plants and their atmospheric environment. *Quart. J. Roy. Meteor. Soc.*, **94**, 523-544.

Donham, K. J., S. Wing, D. Osterberg, J. L. Flora, C. Hodne, K. M. Thu, and P.S. Thome, 2007: Community health and socioeconomic issues surrounding concentrated animal feeding operations. *Environ. Health Perspect.*, **115**, 317-320.

EPA, 2009: 2009 Final Report: Integrated Science Assessment for Particulate Matter. U.S. Environmental Protection Agency EPA/600/R-08/139F, 1071 pp.

Faulkner, W.B., J.M. Lange, J.J. Powell, B.W. Shaw, and C.B. Parnell, 2007: Sampler placement to determine emission factors from ground level area sources. *Atmos. Environ.*, 41, 7672-7678, doi: 10.1016/j.atmosenv.2007.08.029.

Hammond, E.G., C. Fedler, and G. Junk, 1979: Identification of dust-borne odors in swine confinement facilities. *Trans. ASABE,* **22**, 1186-1189.

Hammond, E.G., and R.J. Smith, 1981: Survey of some molecularly dispersed odorous constituents in swine house air, Iowa State Journal of Research, **55**, 393-399.

Hammond, E.G., C. Fedler, and R.J. Smith, 1981: Analysis of particle-borne swine house odors. *Agric. & Environ*., **6**, 395-401.

Hernandez, G., S. Trabue, T. Sauer, R. Pfeiffer, and J. Tyndall, 2012: Odor mitigation with tree buffers: Swine production case study. *Agric., Ecosyst. Environ.,* **149**, 154-163, doi: 10.1016/j.agee.2011.12.002.

Holmén, B. A., W. E. Eichinger, and R. G. Flocchini, 1998: Application of elastic lidar to PM10 emissions from agricultural nonpoint sources. *Environ. Sci. Technol.,* **32**, 3068-3076.

Husar, R. B., and S. R. Falke,1996: The relationship between aerosol light scattering and fine mass. Center for Air Pollution Impact and Trend Analysis (CAPITA) Report 63130-4899, 28 pp, [Available online at http://vigor2.seas.wustl.edu/images/6/66/96j1.pdf.]

Jones, H.W., L. Wang-Li, and B. Y. Boroujeni, 2012: Impact of downwind sampling location and height on inverse-Gaussian dispersion modeling: A theoretical study. *Int. J. Agric. & Biol. Eng.*, **5**, 39-46.

Klett, J. D., 1981: Stable analytical inversion solution for processing lidar returns. *Appl.Opt.,* **20**, 211-220, doi: 10.1364/AO.20.000211.

Klett, J.D., 1985: Lidar inversion with variable backscatter/extinction ratios. *Appl. Opt.,* **24**, 1638-1643, doi: 10.1364/AO.24.001638.

Krichbaumer, W., and Ch Werner, 1994: Current state-of-the-art of LIDAR inversion methods for atmospheres of arbitrary optical density. *Appl. Phys. B: Lasers Opt.,* **59**, 517-523, doi: 10.1007/BF01082394.

Kovalev, V. A., and W. E. Eichinger, 2004: *Elastic lidar: theory, practice, and analysis methods*. John Wiley & Sons, 615 pp.

Lagrosas, N., H. Kuze, N. Takeuchi, S. Fukagawa, G. Bagtasa, Y. Yoshii, S. Naito, and M. Yabuki, 2005: Correlation study between suspended particulate matter and portable automated lidar data. *J. Aerosol Sci.,* **36**, 439-454, doi: 10.1016/j.jaerosci.2004.10.007.

Laird, D.J., 1997: Wind Tunnel Testing of Shelterbelt Effects on Dust Emissions from Swine Production Facilities, M.S. Thesis, Iowa State University.

Lewandowski, P. A., 2009: Advances in Lidar Applications, Diss., The University of Iowa, 101 pp.

Li, Q., and Coauthors, 2013: The national air emission monitoring study's southeast layer site: part II. particulate matter. Trans. ASABE, **56**, 1173-1184.

Lin, X.-J., S. Barrington, J. Nicell, D. Chointière, and A. Vézina, 2006: Influence of windbreaks on livestock odour dispersion plume in the field. *Agric., Ecosyst. Environ.,***116**, 263-272, doi:10.1016/j.agee.2006.02.014.

MacDonald, J.M., and W.D. McBride, 2009: The Transformation of U.S. Livestock Agriculture: Scale, Efficiency, and Risks. Economic Information Bulletin No. 43, Economic Research Service, USDA, 46 pp.

Malone, G., G. VanWicklen, S. Collier, and D. Hansen, 2006: Efficacy of vegetative environmental buffers to capture emissions from tunnel ventilated poultry houses. *Proc. Workshop Agric. Air Qual.*, Washington, D.C., 875-878. [Available online at http://www.umad.de/infos/woaaq2006/Posters-M.pdf.]

Monin, A.D. and A.M. Obukhov, 1954: Basic Laws of Turbulent Mixing in the Surface Layer of the Atmosphere. *Geophys. Inst. Acad. Sci. USSR,* **24**,163-187.

Murphy, D.M., D.J. Cziczo, P.K. Hudson, M.E. Schein, and D.S. Thomson, 2004: Particle density inferred from simultaneous optical and aerodynamic diameters sorted by composition. *J. Aerosol Sci.* **35**, 135–139, doi: 10.1016/S0021-8502(03)00386-0.

National Research Council (NRC), Ad Hoc Committee on Air Emissions from Animal Feeding Operations, 2003: Air emissions from animal feeding operations: current knowledge, future needs. National Academies Press, 264 pp. [Available online at http://www.nap.edu/catalog/10586/air-emissions-from-animal-feeding-operations-current-knowledge-future-needs.]

Ni, J., 2015: Research and demonstration to improve air quality for the US animal feeding operations in the 21st century–A critical review. *Environ. Pollut.,* **200**, 105-119, doi: 10.1016/j.envpol.2015.02.003.

Parker, D. B., G. W. Malone, and W. D. Walter, 2012: Vegetative environmental buffers and exhaust fan deflectors for reducing downwind odor and VOCs from tunnel-ventilated swine barns, *Trans. ASABE,* **55**, 227-240, doi: 10.13031/2013.41250.

Prueger, J.H., W.E. Eichinger, L.E. Hipps, J.L. Hatfield, and D.I. Cooper, 2008: Air-flow distortion and turbulence statistics near an animal facility, *Atmos. Environ.*, **42**, 3301-3314, doi: 10.1016/j.atmosenv.2007.08.048.

Schiffman, S.S., J.M. Walker, P. Dalton, T.S. Lorig, J.H. Raymer, D. Shusterman, and C.M. Williams, 2000: Potential Health Effects of Odor from Animal Operations, Wastewater Treatment, and Recycling of Byproducts. *J. Agromedicine.,* **7**, 7-81, doi: 10.1300/J096v07n01_02.

Stanhill, G, 1969: A simple instrument for the field measurement of turbulent diffusion flux. *J. Appl. Meteorol.,* **8**, 509-513.

Thernelius, S.M, 1997: Wind tunnel testing of odor transportation from swine production facilities. M.S. Thesis, Dept. of Aerospace Engineering, Iowa State University, 121 pp.

Tyndall, J.C., 2009: Characterizing pork producer demand for shelterbelts to mitigate odor: An Iowa case study. Agroforestry Syst, **77**, 205-221, doi: 10.1007/s10457-009-9242-x.

Tyndall, J. and J. Colletti, 2007: Mitigating swine odor with strategically designed shelterbelt systems: a review. *Agroforestry Syst.,* **69**, 45-65, doi: 10.1007/s10457-006-9017-6.

USDA NRCS. 2007: Windbreak plant species for odor management around poultry production facilities. Maryland Plant Materials Technical Note, No. 1, 21 pp [Available online at http://www.plant-materials.nrcs.usda.gov/pubs /mdpmctn7166.pdf.]

Wang, H., and J. Walter, 1987: Particule Density Correction for the Aerodynamic Particle Sizer. *Aerosol Sci. Technol.,* **6**, 191-198, doi: 10.1080/02786828708959132.

Wang-Li, L., 2013: Techniques for characterization of particulate matter emitted from animal feeding operations, *Evaluating Veterinary Pharmaceutical Behavior in the Environment*, G.P. Cobb and P.N. Smith, Ed., Amer. Chem. Soc., 15-39.

Wang-Li, L., Z. Chao, M. Buser, D. Whitelock, C.B. Parnell, and Y. Zhang, 2013: Techniques for measuring particle size distribution of particulate matter emitted from animal feeding operations. *Atmos. Environ.,* **66**, 25-32, doi:10.1016/j.atmosenv.2012.08.051.

Wanjura, J. D., C.B. Parnell, Jr., B.W. Shaw, and R.E. Lacey, 2005: Design and evaluation of a low-volume total suspended particulate sampler. *Trans. ASAE* **48**, 1547-1552.

Wing, S., R.A. Horton, S.W. Marshall, K. Thu, M. Tajik, and S.S. Schiffman, 2008: Air pollution and odor in communities near industrial swine operations. *Environ. Health Perspect,.* **116**, 1362-1368.

Yang, X., Y. Lorjaroenphon, K.R. Cadwallader, X. Wang, Y. Zhang, and J. Lee, 2014: Analysis of particle-borne odorants emitted from concentrated animal feeding operations. *Sci. Total Environ.,* **490**, 322-333, doi: 10.1016/j.scitotenv.2014.05.026.

Zirschky, J., 1985: Geostatistics for environmental monitoring and survey design. *Environ. Int.*, 11, 515-524.

APPENDIX

Table A1. 2-dimensional concentration and mass maps for each run.

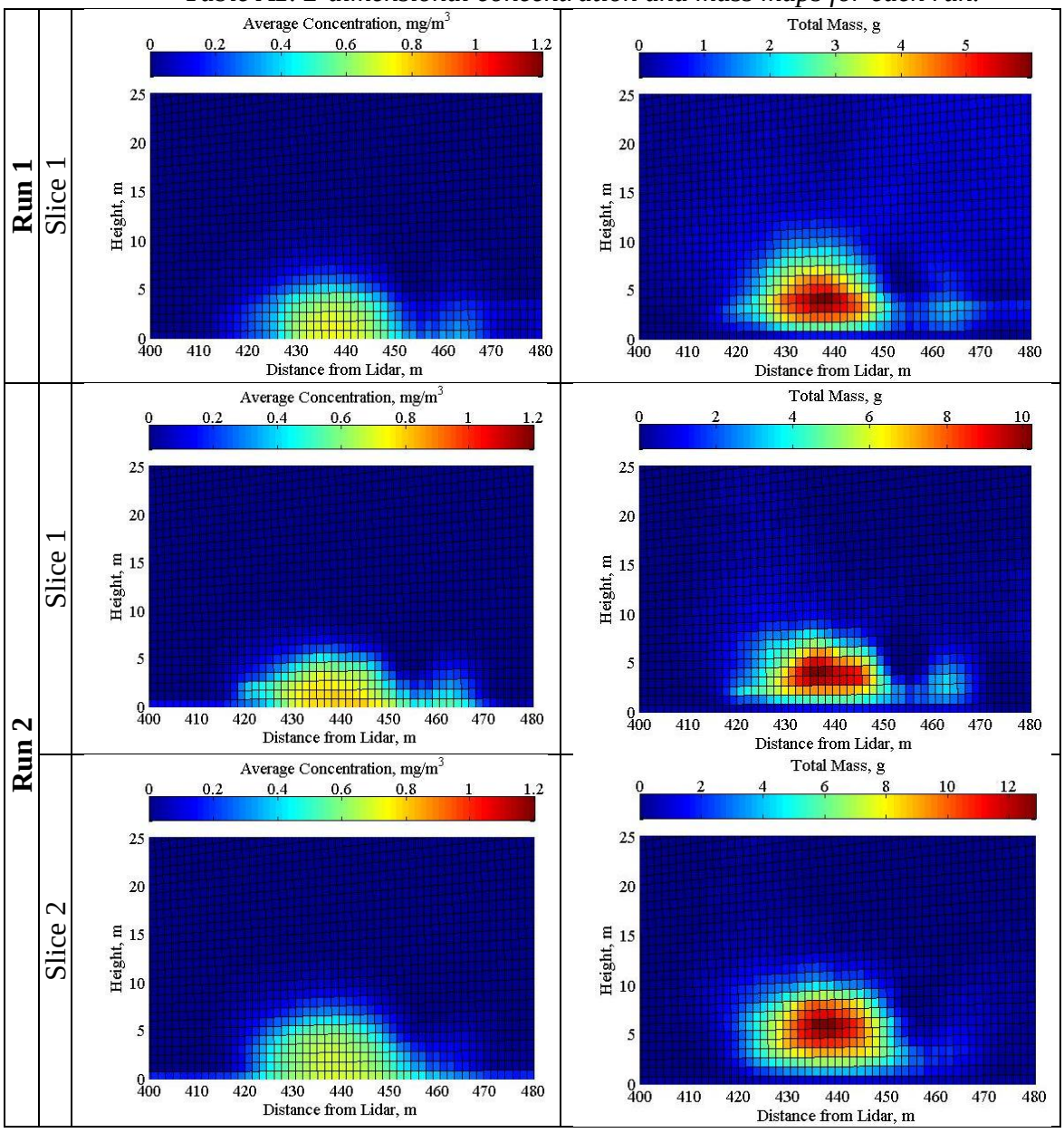

Table A1 - continued.

Run 3	Slice 1	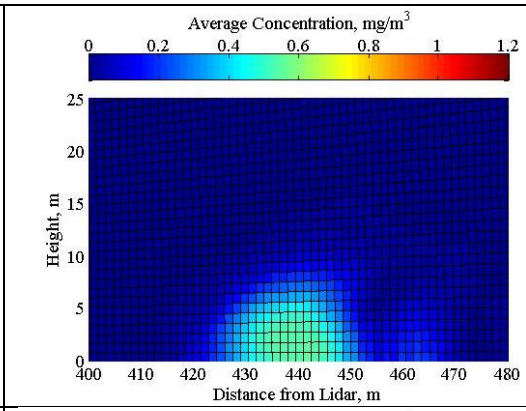	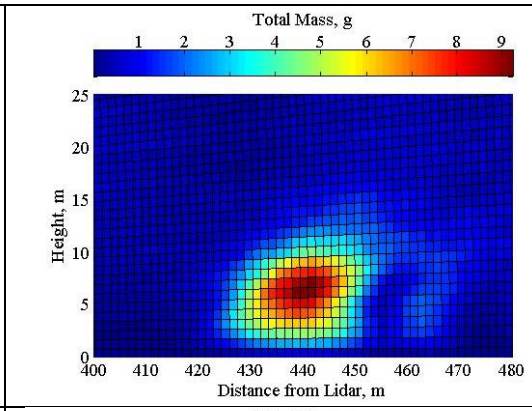
	Slice 2	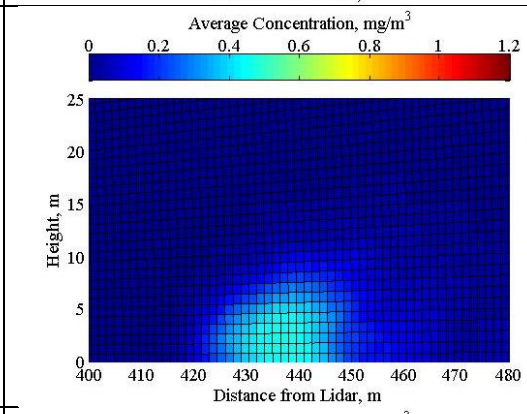	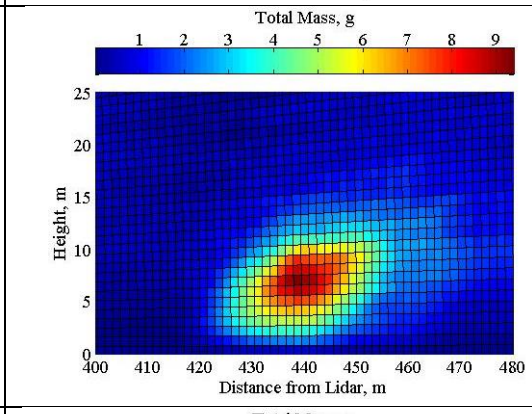
Run 4	Slice 1	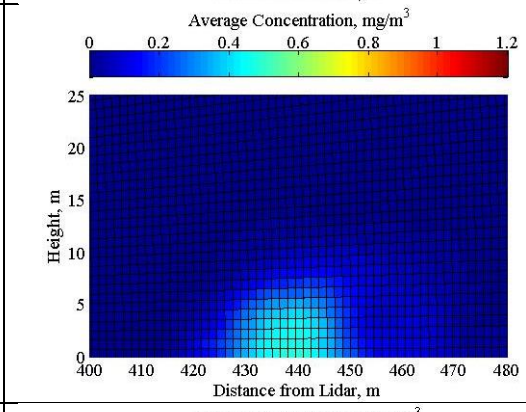	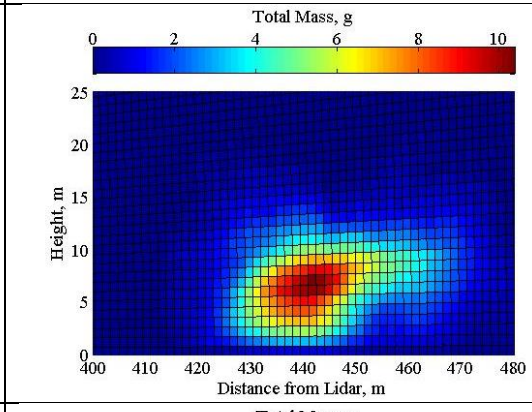
	Slice 2	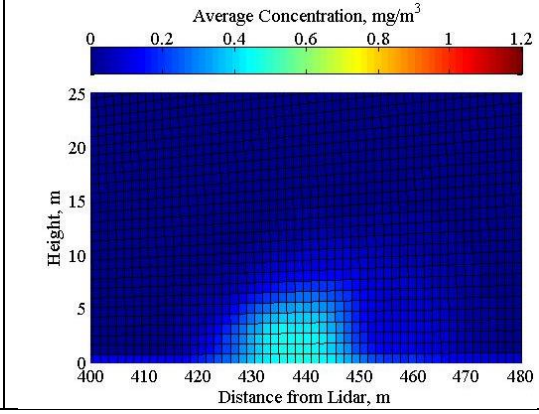	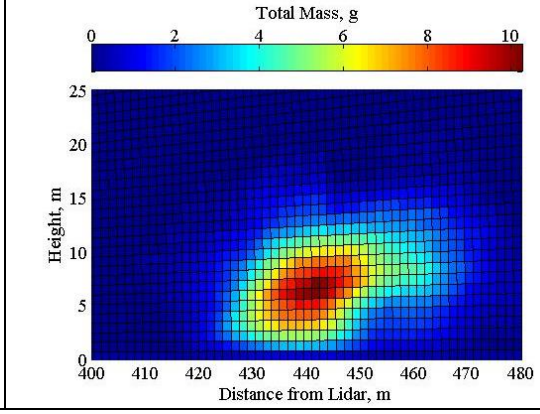

Table A1 - continued.

Run 5	Slice 1	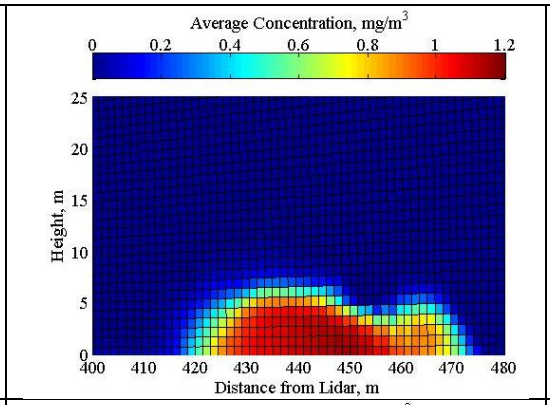	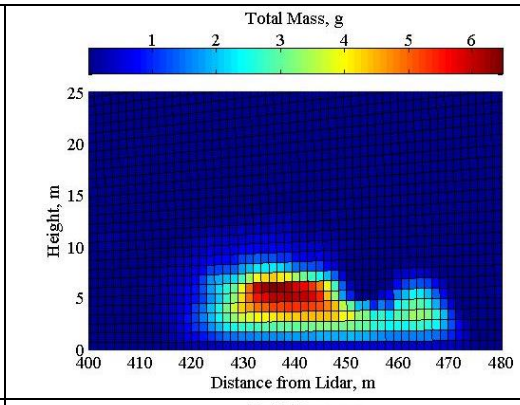
	Slice 2	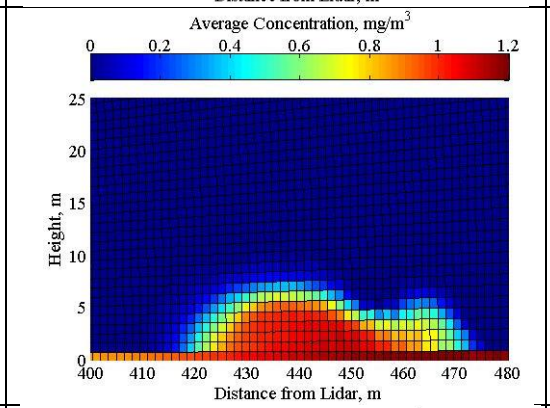	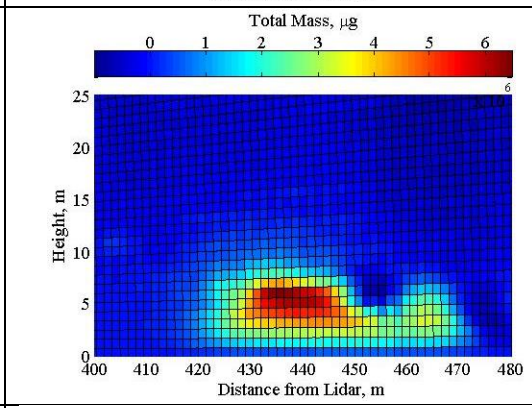
Run 6	Slice 1	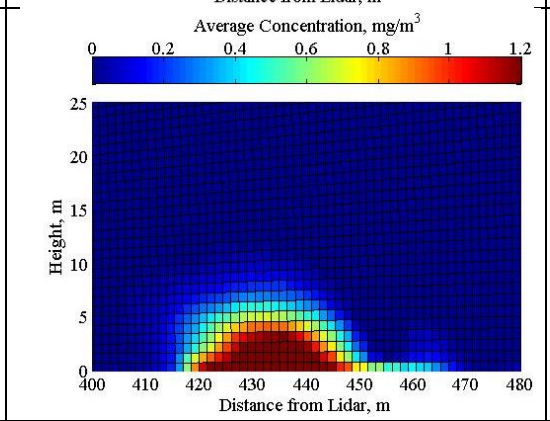	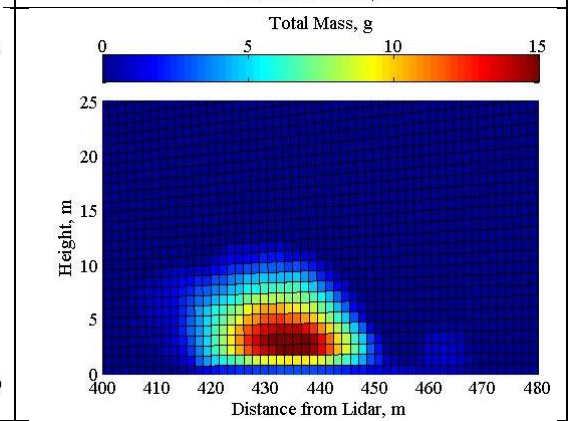
	Slice 2